Observation of rotation about the longest principal axis in ^{89}Zr

S. Saha, R. Palit, J. Sethi, S. Biswas, P. Singh, S. Nag, A. K. Singh, I. Ragnarsson, F. S. Babra, U. Garg, A. Goswami, E. Ideguchi, H. C. Jain, S. Kumar, Md. S. R. Laskar, G. Mukherjee, Z. Naik, and C. S. Palshetkar

Observation of rotation about the longest principal axis in ^{89}Zr

S. Saha[1,2,3],* R. Palit[1],† J. Sethi[1], S. Biswas[1], P. Singh[1], S. Nag[4], A. K. Singh[5], I. Ragnarsson[6], F. S. Babra[1], U. Garg[7], A. Goswami[8‡], E. Ideguchi[9], H. C. Jain[1], S. Kumar[10], Md. S. R. Laskar[1], G. Mukherjee[11], Z. Naik[12], and C. S. Palshetkar[1]

[1] *Department of Nuclear and Atomic Physics, Tata Institute of Fundamental Research, Mumbai 400005, India*
[2] *GSI Helmholtzzentrum für Schwerionenforschung GmbH, Darmstadt 64291, Germany*
[3] *Technische Universität Darmstadt, Darmstadt 64289, Germany*
[4] *Department of Physics, Indian Institute of Technology (Banaras Hindu University), Varanasi 221005, India*
[5] *Department of Physics, Indian Institute of Technology Kharagpur, Kharagpur 721302, India*
[6] *Division of Mathematical Physics, LTH, Lund University, P.O. Box 118, SE-22100 Lund, Sweden*
[7] *Physics Department, University of Notre Dame, Notre Dame, Indiana 46556, USA*
[8] *Saha Institute of Nuclear Physics, Kolkata 700064, India*
[9] *Research Center for Nuclear Physics (RCNP), Osaka University, Osaka 567-0047, Japan*
[10] *Department of Physics and Astrophysics, University of Delhi, Delhi 110007, India*
[11] *Variable Energy Cyclotron Centre 1/AF Bidhan Nagar, Kolkata 700064, India and*
[12] *Physics Department, Sambalpur University, Sambalpur-768019, India*

High-spin states in ^{89}Zr were populated in the ^{80}Se(^{13}C,4n) reaction and γ-ray coincidences were measured using the INGA spectrometer. The level scheme of ^{89}Zr has been extended up to spin $I = 49/2$ with the observation of a new dipole band. Directional Correlation and polarization asymmetries of the γ rays have been measured to determine spin and parity of the levels. Line shapes of several transitions have been analyzed to determine lifetimes of the levels. Possible configurations of the band have been discussed using cranked Nilsson Strutinsky model. The calculations suggest triaxial shape of the nucleus at high spins and the band may represent rotation of the nucleus about the longest axis.

PACS numbers:

I. INTRODUCTION

The structure of the high-spin states of nuclei near closed shells is a subject of considerable interest for the study of the emergence of collectivity. While the low-lying states of these nuclei are dominated by single-particle excitation, collective rotational structure may emerge due to the occupation of high-j orbitals at higher excitation energy. Recently, deformed band structures have been observed in the doubly magic ^{40}Ca and ^{56}Ni nuclei at high spins [1, 2]. Theoretical calculations predict that the collective excitations are due to multiple particle-hole excitations across the major shell gap. For example, 8p-8h and 4p-4h excitations have been observed across the respective shell gaps in ^{40}Ca and ^{56}Ni [1, 2]. These observations have made the doubly magic nuclei a searching ground for onset of collectivity at high spins in recent times. However, high-spin states of heavier doubly closed shell nuclei beyond ^{56}Ni are difficult to observe experimentally.

The low ground state deformation in nuclei close to ^{90}Zr makes them ideal candidates to study evolution of deformed shape with increasing spin. The $Z = 40$ sub-shell closure and $N = 50$ major shell closure make the system analogous to a doubly closed shell nucleus. At high spin the effect of pairing correlations is expected to get reduced, whereas the Coriolis effect can drive the high-j orbitals to lower energies. This enhances the possibility of neutron excitations from the $g_{9/2}$ to the $d_{5/2}$ orbitals at higher angular momentum. Theoretical calculations show that the collectivity in a nucleus is expected to get enhanced by the interplay of the quadrupole force with the central field in a major shell spanned by the sequence of $\Delta j = 2$ orbitals that comes lowest under the spin-orbit splitting [3]. Moreover, recent works also predict Jacobi like shape transition in ^{90}Zr [4, 5].

In this region of the nuclear landscape, regular dipole band structures have been observed at high spins in ^{88}Sr [6], ^{86}Kr and ^{89}Y [7, 8] nuclei. These band structures have been successfully described involving excitations of protons to the $g_{9/2}$ orbital and neutrons to the $d_{5/2}$ orbital across the N=50 shell closure. One of the common characteristics of these bands is enhanced $M1$ strengths with very weak or completely suppressed $E2$ crossovers. With the motivation to look for regular band structures, high-spin states of ^{89}Zr have been studied and lifetime measurements of some of the observed levels have been carried out in the present work.

The article is organized as follows: The experimental details are given in the Section II, whereas in the Section III the experimental results are discussed. The experimental observations and the theoretical calculations are compared in Section IV. Section V briefly summarizes the work reported in the manuscript.

‡Deceased.
*Corresponding Author: `s.saha@gsi.de`
†Corresponding Author: `palit@tifr.res.in`

II. EXPERIMENTAL DETAILS AND ANALYSIS PROCEDURE

Excited states of ^{89}Zr were populated using the ^{80}Se(^{13}C,4n) reaction in two experiments. In the first experiment, a beam of ^{13}C at a laboratory energy of 50 MeV impinged a 800-$\mu g/cm^2$ ^{80}Se target with a thick (10 mg/cm^2) ^{197}Au backing. The second experiment, aimed at accessing higher spins, used a higher beam energy (60 MeV) on the ^{80}Se target (500 $\mu g/cm^2$ on a 80-$\mu g/cm^2$ Al backing). In this second experiment, the target was reverse mounted with the Al backing facing the incident beam. The γ rays emitted in the reaction have been measured with the Indian National Gamma Array (INGA) at TIFR which is a Compton suppressed clover detector array with a provision of placing 24 clovers at various angles with respect to the beam direction. In the present configuration, four clover detectors were kept at 90°, three detectors each at 40°, 115°, 140°, 157°, and two detectors at 65°. The time stamped data were collected with two- and higher-fold coincidence condition using an XIA based digital data acquisition system [11]. The data were sorted using an offline analysis code "MARCOS" to generate a $\gamma - \gamma$ matrix and a $\gamma - \gamma - \gamma$ cube [12]. Both the matrix and the cube events were analyzed to search for the new γ rays at high spin. Angle dependent matrices were also generated and used for the analysis of the directional correlation of oriented states (R_{DCO}) and doppler shift attenuation measurements.

Using the data from the first experiment, the level scheme could be extended up to 8106 keV and 9602 keV excitation energies for negative and positive parity states, respectively [9]. In the present work, lifetimes of some of the states above the 6244-keV level were extracted using doppler shift attenuation technique. In the second experiment, the ^{80}Se target was thin enough so that recoiling residues produced in the fusion evaporation reaction could escape the target material. The γ rays emitted from the residual nuclei will have constant Doppler shift at any given angle due to uniform in-vacuum velocity of the residues. For each clover detector, the Doppler shift of the γ rays was corrected using the velocity of the recoil and the angle subtended by the clover to the beam direction.

The spin and parity of the levels were assigned using R_{DCO} [13, 14] and polarization asymmetry measurements [15, 16], respectively. For R_{DCO} measurement, asymetric matrices were made with events detected in detectors at 157° on one axis and those detected in detectors at 90° on the other axis. The matrices were updated with events collected within a coincidence window of 150 ns. The R_{DCO} values were extracted using the formula:

$$R_{DCO} = \frac{I(\gamma_1) \text{ at } 157° \text{gated by } \gamma_2 \text{ at } 90°}{I(\gamma_1) \text{ at } 90° \text{gated by } \gamma_2 \text{ at } 157°} \quad (1)$$

where, I(γ_1) represents intensity of γ_1 measured in coincidence with γ_2. The DCO ratio values for a stretched dipole and quadrupole transition gated by a pure quadrupole (dipole) transition are $\sim 0.5(1.0)$ and $\sim 1.0(2.0)$, respectively.

The polarization asymmetry, Δ, was extracted from parallel ($N_{\parallel}$) and perpendicular ($N_{\perp}$) scattered events detected in the 90° clovers in coincidence with γ-rays detected at any other angle using the following relationship [17]:

$$\Delta = \frac{a(E_\gamma)N_{\perp} - N_{\parallel}}{a(E_\gamma)N_{\perp} + N_{\parallel}} \quad (2)$$

where, $a(E_\gamma)$ is a correction factor for the parallel to perpendicular scattering asymmetry within the crystals of a clover. The value of $a(E_\gamma)$ for the 90° clover detectors is 1.00(1) [18]. The positive and the negative values of Δ represent electric and magnetic transitions, respectively.

III. RESULTS

The positive- and negative-parity states of ^{89}Zr were established in the previous work using a Au-backed target [9]. With the observation of a new band in this experiment, the negative-parity states of the level scheme have been extended up to ~ 12 MeV in excitation energy and $(49/2^-)$ $\hbar$ spin.

A number of new transitions have been observed in the present experiment which were otherwise poorly visible in the previous thick-target data. By putting different gate combinations in the cube and the matrix seven new γ-ray transitions with energies 517-, 525-, 597-, 604-, 612-, 668- and 718-keV have been observed to be in coincidence with themselves. The new γ rays are shown in Fig. 1, where in panel (a) coincidence gate on 215-keV transition is applied on the $\gamma - \gamma$ matrix to generate the spectrum. The spectrum depicted in panel (b) of Fig. 1, is generated by a double-coincidence gate on 589- and 675-keV γ-ray transitions applied to the $\gamma - \gamma - \gamma$ cube data. The energies of all the transitions belong to the dipole band are shown with asterix. The reduction in population of the levels with increase in angular momentum could be observed from the intensity of the γ-rays in the spectrum. Weak crossover γ rays of 1264-, 1183- and 1025-keV energies have also been observed across the 589-675 keV, 675-508 keV and 508-517 keV transitions, respectively. Other transitions in the level scheme such as 525-, 597-, 604-, 612-, 668- and 718-keV γ rays, are placed with decreasing intensity. All intensities are obtained from 215 keV gated spectrum and normalised to 589-keV [9] transition. Since the energy of 508-keV transition is very close to 511 keV annihilation γ-ray, a possibility of doublet 508 keV could not be ruled out and an upper limit of the intensity of this γ-ray transition is provided in Table I.

Polarization asymmetries have been determined for the 589-, 675-, 508-, 517- and 525-keV transitions. All these transitions have small negative polarization asymmetry

values (see Table I). The 675-keV transition with DCO value 0.54(8) and asymmetry -0.05(2), as obtained from previous experiment, suggest pure $M1$ character for this transition. Hence, this transition is used as a gate for extracting the DCO ratios of all the other transitions of the band. The measured DCO ratios of the 589-, 508-, 517- and 525-keV transitions are ~ 1 in the 675 keV dipole gate. Hence, the multipolarity of these transitions can be assigned as $\Delta I = 1$. The DCO value of the 517 keV transition has been found to be 1.46(5) in 675-keV gate, which indicates $E2$ admixture in this transition. The 597-, 604-, 612-, 668- and 718-keV γ rays of the cascade have been tentatively assigned as $M1$ transitions. This makes spins of the levels tentative. A partial level scheme of ^{89}Zr above the 6074-keV state is shown in Fig. 2. The intensities, DCO and polarization asymmetry values of the observed γ-rays have been shown in Table I.
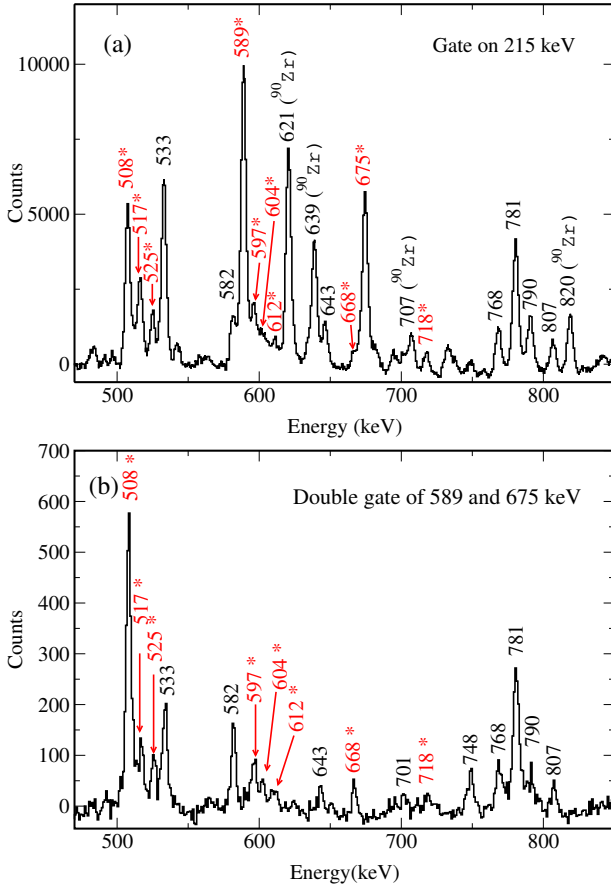

FIG. 1: (Color online) In panel (a) a coincidence spectrum with gate on 215 keV [9] transition is shown, while in panel (b) double coincidence spectrum with gates on 589- and 675-keV is presented. The transitions energies (in red) marked with asterix belong to the negative parity band discussed, while other γ-rays are either belong to ^{89}Zr [9] or from ^{90}Zr level scheme.

Lifetimes of some of the states have been determined from the experiment with Au-backed target [9]. Two
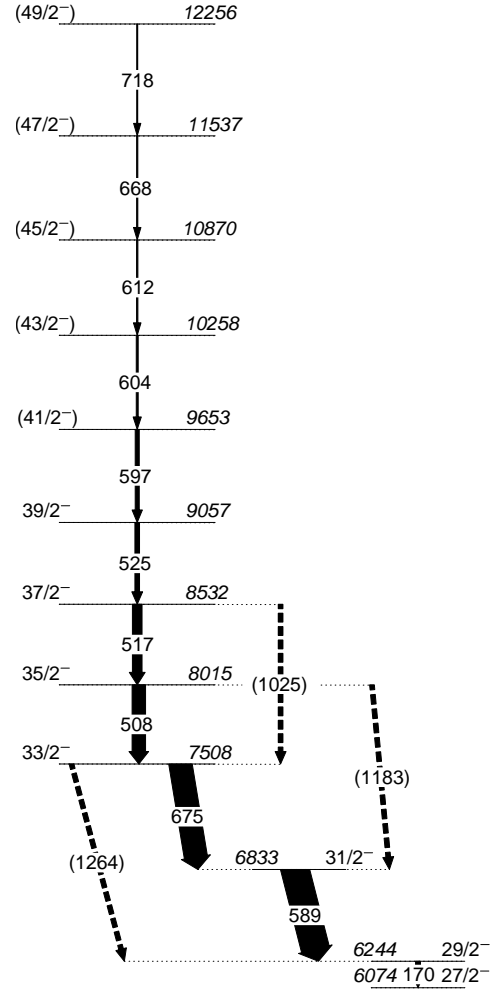
FIG. 2: Partial level scheme of ^{89}Zr showing a regular structure of $M1$ transitions above $I^{\pi} = 29/2^-$. The thickness of the vertical arrows representing γ rays is proportional to the intensity of the corresponding γ ray.

angle-dependent asymmetric γ-γ matrices (all vs 40° and all vs 140°) were formed for the line shape analysis.

The Doppler-shifted spectra were generated from the asymmetric matrices with a gate on 533-keV γ ray (not shown in the partial level scheme given in Fig. 2) [9], a dipole transition decaying out of the band. Representative lineshape spectra of 589- and 675-keV transitions observed at 40° and 140° angles are displayed in Fig. 3. Lifetimes of the excited levels were extracted using the program LINESHAPE [19]. Energy loss of the projectile as well as of the recoil through the target material was calculated using shell-corrected Northcliffe and Schilling stopping powers [20]. A Monte Carlo simulation of 5000 histories of nuclei recoiling through target and backing materials with a time step of 0.01 ps were generated by the "dechist "and "histaver "programs. Independent one step side feeding has been considered instead of a rotational cascade feeding the band. With decreasing excitation energy of the level an increase of the side-feeding

TABLE I: Excitation energies of levels (E_i), inital and final spin ($I_i^\pi \to I_f^\pi$), γ-ray energies (E_γ), intensities (I_γ), R_{DCO} and polarization asymmetry (Δ) of γ-ray transitions belonging to the negative parity dipole band of ^{89}Zr. The data are deduced from the experiment using the thin Al-backed target. The intensities of the γ rays have been normalized to that of the 589.0-keV transition measured in the thick-target experiment [9]. The uncertainties in the energies of the gamma rays are 0.3 keV for intense gamma rays and 0.7 keV for the weak transitions.

E_i (keV)	$I_i^\pi \to I_f^\pi$	E_γ (keV)	I_γ	R_{DCO}[†]	Δ
6833 .0	$31/2^- \to 29/2^-$	589.0	6.06(32)	1.12(2)[a]	-0.09(1)
7507.7	$33/2^- \to 31/2^-$	674.7	4.96(3)	0.97(2)[c]	-0.04(2)
8015.2	$35/2^- \to 33/2^-$	507.5	<4.10(5)[d]	0.87(2)[a]	-0.05(1)
8531.7	$37/2^- \to 35/2^-$	516.5	2.05(12)	1.46(5)[a]	-0.02(3)
9056.5	$39/2^- \to 37/2^-$	524.8	0.98(7)	1.14(6)[a]	-0.04(1)
9653.3	$(41/2^-) \to 39/2^-$	596.8	0.86(6)	—	—
10257.5	$(43/2^-) \to (41/2^-)$	604.2	0.41(5)	—	—
10869.8	$(45/2^-) \to (43/2^-)$	612.3	0.28(3)	—	—
11537.3	$(47/2^-) \to (45/2^-)$	667.5	0.25(4)	—	—
12255.7	$(49/2^-) \to (47/2^-)$	718.4	0.21(3)	—	—

[†]R_{DCO} has been obtained with gate indicated through prefix of the R_{DCO} values.
[a] From 675 keV ($M1$) DCO gate.
[c] From 589 keV ($M1$) DCO gate.
[d] The possibility of another 507.5 keV could not be ruled out. Therefore, only upper limit on intensity is quoted here.

TABLE II: Excitation energy of the decaying state(E_i), spin-parity (I_i^π), γ-ray transition energy($E_{\gamma,M1}$), lifetime (τ) and $B(M1)$ values for a few states of ^{89}Zr.

E_i (keV)	I_i^π	$E_{\gamma,M1}$ (keV)	τ (ps)	$B(M1)$ $(\mu_N)^2$
6833.0	$31/2^-$	589.0	$0.14^{+0.02}_{-0.02}$	$1.96^{+0.32}_{-0.25}$
7507.7	$33/2^-$	674.7	$0.15^{+0.01}_{-0.01}$	$1.26^{+0.12}_{-0.11}$
8015.2	$35/2^-$	507.5	$0.30^{+0.01}_{-0.02}$	$1.44^{+0.10}_{-0.06}$
8531.7	$37/2^-$	516.5	$0.42^{+0.08}_{-0.07}$	$<0.99^{+0.21}_{-0.15}$ [a]
9056.5	$39/2^-$	524.8	<0.21	>1.86

[a] DCO value of 517 keV transition in 675 keV gate (given in Table. I) indicates its M1+E2 nature. Therefore, upper limit on B(M1) value has been quoted here.

times has been assumed according to Ref. [21].

In the fitting process, the lineshapes of 589- and 675-keV transitions were fitted separately in different windows while those for 508-, 517- and 525-keV γ rays were fitted together in the same window as they had significant overlap at forward and backward angles. Fittings were carried out for lineshape observed in detectors at 65°, 115° and 90° as the nearby transitions show larger overlap at other angles. The level lifetimes and their errors reported in Table II are obtained from the lineshape fitting of the the angle dependent doppler shifted spectra at these angles.

A proper estimation of the background and contamination peaks were made before fitting of calculated lineshapes with the experimental ones. The 9057-keV level with $I^\pi = 39/2^-$ is the topmost state for which lifetime could be extracted in this experiment. A 100% side feeding intensity was considered for this level. For the lower levels, the difference of measured intensities of the γ-ray transitions populating and depopulating the level of interest was used as an initial sidefeeding intensity parameter for the fit. The side-feeding intensities were obtained from the detectors placed at 90°. After the χ^2 minimization from the MINUIT [22] program, the background and the contaminant peak parameters were fixed and the procedure was followed for the next lower level. In addition, a global fit for all the transitions of the cascade was carried out keeping the background and the contaminant peak parameters fixed. The lifetimes of various states as obtained from the LINESHAPE code along with the $B(M1)$ values are listed in Table II. The errors quoted in lifetimes do not include the systematic errors from the uncertainty in stopping power, which can be as large as 15% [23].

IV. DISCUSSION

The microscopic structure of nuclei in the $Z \approx 40$, $N \approx 50$ region is governed by the occupation of the $1g_{9/2}$, $2p_{1/2}$, $1f_{5/2}$, $2d_{5/2}$, $1g_{7/2}$ and $1h_{11/2}$ orbitals. The $d_{5/2}$, $g_{7/2}$ and $h_{11/2}$ neutron single-particle orbitals are
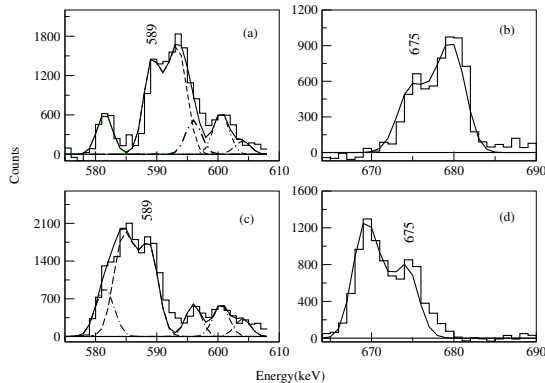
FIG. 3: Representative spectra (with gate on the lower transition) along with fitted line shapes for 589- (panels (a) and (c)) and 675-keV (panels (b) and (d)) transitions of ^{89}Zr. The upper panels, (a) and (b), show γ-ray spectra observed at 40° and panels (c) and (d) for detectors at 140°. The calculated Doppler shifted lineshapes are shown in dashed lines, whereas the total lineshape, and contamination peaks are shown with solid, and dash-dot lines, respectively.

strongly downsloping when they are drawn versus prolate deformation, which means that their occupation will drive the nucleus towards prolate shape. Owing to low level density in $A \sim 90$ compared to $A \sim 160$ region, the nuclei in this mass region are known to show larger shape variation effects with respect to change in particle number as well as spin.

In one of our earlier publications, Ref. [9], the experimentally observed negative parity states (populated up to $37/2$ $\hbar$ and 10 MeV) in ^{89}Zr were investigated in the framework of shell model. The calculations were carried out using JUN45 [24, 25] and jj44b [26] interactions optimized within the model space comprising of $f_{5/2}$, $p_{3/2}$, $p_{1/2}$ and $g_{9/2}$ orbitals. The shell model calculations using both interactions have been found to be progressively overestimating the experimental levels of the band beyond $37/2$ $\hbar$. This indicates that the spin states up to $I = 37/2$ $\hbar$ can be constructed with a few protons excited from the fp shell to the $g_{9/2}$ orbital and with no excitation across the $N = 50$ core. In fact, other $N = 48$ isotones, such as ^{86}Sr [27], ^{88}Zr [18] and ^{90}Mo [28], are known to show shell model type excitations. Higher spin states are expected to be built with a contribution from neutron excitations since exciting too many protons beyond $Z = 40$ is not energetically favorable. In this mass region, ^{90}Mo is an example where states up to $I = 25$ $\hbar$ could be populated [28]. These states have been assigned a configuration $(\pi(g_{9/2}^4)(\nu(g_{9/2}^{-3}d_{5/2}))$ with excitation of neutrons beyond $N = 50$, but no rigorous calculation was presented in support of the argument [28]. Similarly, in $N = 50$ isotones such as ^{88}Sr [6], ^{86}Kr [7] and ^{90}Zr [29], the configuration based on neutron excitation across N

= 50 shell gap has been suggested for high-spin states using large scale shell-model calculations.

High-spin states can be described using the cranking approach [30, 31], where the nucleons are assumed to be moving freely in a deformed mean field as described for example by the modified oscillator (Nilsson) potential [32]. In the configuration dependent cranked Nilsson Strutinsky (CNS) approach [33–36], the total energy of the nucleus at a specific deformation is parameterized by ε_2, ε_4 and γ [33, 37] and the energy can be written as a sum of a rotating liquid drop energy (E_{RLD}) and the shell energy (E_{sh}). The Lublin-Strasbourg Drop (LSD) model [38] is used to calculate the macroscopic energy with the rigid body moment of inertia calculated with a radius parameter of $r_0 = 1.16$ fm and a diffuseness of $a = 0.6$ fm [36]. An energy scale based on mass excess is employed which makes it possible to compare high-spin states in different nuclei.

The Nilsson parameters κ and μ defining the $l \cdot s$ and l^2 strengths of the modified oscillator potential appear rather uncertain in this region of nuclei. The so-called $A = 80$ parameters [39] have been used in high spin studies of several nuclei in the vicinity of ^{89}Zr, e.g. ^{87}Nb [40], ^{86}Zr [41] and ^{84}Zr [42]. These parameters and some other fits are discussed in Ref. [43]. It would be interesting to try these fits and to test the trends which are discussed in Ref. [43], but the present data on ^{89}Zr are too limited to make such a comparison meaningful. Therefore, we have used the $A = 80$ parameters [39], which are defined as follows:

For $\mathcal{N} = 3$: κ_p=0.065, μ_p=0.40, κ_n=0.07, μ_n=0.40
For $\mathcal{N} = 4$: κ_p=0.075, μ_p=0.40, κ_n=0.08, μ_n=0.40
For $\mathcal{N} \neq 3,4$: κ_p=0.080, μ_p=0.30, κ_n=0.08, μ_n=0.22

Here, $\mathcal{N}$ is the oscillator shell quantum number and $\kappa_p(\kappa_n)$ and $\mu_p(\mu_n)$ denote the coupling strengths of the $l \cdot s$ and l^2 terms for protons and neutrons. The CNS model does not include pairing correlations and hence, the calculated results are mainly relevant for high-spin states.

In the CNS model, for each major shell $\mathcal{N}$ within a rotating basis of the Nilsson potential, the single-particle states are grouped into high-j and low-j orbitals. The neglect of pairing makes it possible to define configurations in a detailed way, fixing the number of particles occupying orbitals of high-j and low-j character, respectively, in the different $\mathcal{N}$-shells. The nomenclature followed in the present study to label the configurations is

$$[p_1p_2, n_1n_2n_3],$$

defining the number of particles and holes relative to a ^{90}Zr core. Thus, p_1 is the number of proton holes in the fp shell and p_2 represents the number of protons in the $g_{9/2}$ shell. Furthermore, n_1 is the number of neutron holes in $g_{9/2}$ shell, n_2 corresponds to the number of neutrons occupying $d_{5/2}$ and $g_{7/2}$ (gd) orbitals and n_3 the number of $h_{11/2}$ neutrons. For a complete description of

a configuration, the signature in the subshells or group of subshells must be specified. Thus, for an odd number of particles in a group, the signature might be given by a subscript, + for signature $\alpha = 1/2$ and $-$ for $\alpha = -1/2$, while it is assumed that $\alpha = 0$ for an even number of particles.

Calculations were performed to probe into energetically favored configurations which are best suited to describe the observed negative parity band in ^{89}Zr. In the calculations, the total energy of the nucleus is minimized at each spin with respect to deformation parameters. The calculated lowest energy negative parity configurations are shown in Fig. 4.

FIG. 4: (Color online) Calculated excitation energy relative to a rotating liquid drop energy as a function of spin for negative parity states in ^{89}Zr. The closed and the open circles represents the ($\alpha = 1/2$) and the ($\alpha = -1/2$) states respectively. The yrast lines for the two signatures are shown by brown dashed lines. Aligned states are encircled. With increasing spin, configurations become yrast which have more and more particles excited across the $Z = 40$ and $N = 50$ gaps, and thus a higher spin content. For the [33,210] configuration, which is assigned to the observed dipole band, all 8 signature combinations are displayed while only the configurations which are low in energy are shown for other configurations.

With increasing spin, more and more particles will be excited across the Fermi level so that higher spin states become yrast. As can be seen in Fig. 4, configurations with one proton in $g_{9/2}$ are the lowest negative parity states at low spin up to 11.5 $\hbar$ which is the highest spin that can be built in these configurations. This is in line with the shell model calculations [9] where also higher spin negative parity states are built as in the present CNS calculations, namely with three protons excited to the $g_{9/2}$ shell. These configurations have a maximum spin

of 19.5 $\hbar$, which is clearly below the highest spin observed experimentally. However, if a neutron is excited across the $N = 50$ shell, i.e. a [33, 210] or $(\pi((fp)^{-3}g_{9/2}^3) \otimes \nu(g_{9/2}^{-2}(dg)^1))$, the configuration becomes yrast up to (and beyond) the spin values observed in the dipole band.

In order to form negative parity states at even higher spin values, either the excited neutron is placed in the $h_{11/2}$ shell combined with four protons excited across the $Z = 40$ gap, [44,320], or two neutrons are excited combined with the excitation of three protons, [33,320]. However, these configurations are calculated approximately 2 MeV higher in energy than the [33,210] configuration. Thus, it appears very safe to conclude that the observed dipole band is built from the [33,210] configuration.

The configuration [33,210] has been investigated in detail in CNS with different combinations of signatures. Because there is an odd number of particles in three groups of orbitals, there are 2^3 signature combinations which are all displayed in Fig. 4. The observed dipole band develops smoothly with spin which means that we should find calculated configurations which show a smooth trend with increasing spin and which are low in energy at high spin where the band is populated. This, clearly suggests that the even spin states of the observed band should be assigned to the $[3_+3_+, 21_-0]$ configuration which behaves smoothly in an extended spin range $I = 12.5 - 22.5$ and which is the lowest energy even spin [33,210] configuration at higher spin values. It then appears that the signature $\alpha = -1/2$ spin sequence should be assigned to the $[3_+3_+, 21_+0]$ configuration, i.e. with a different signature for the dg neutrons. This signature combination is clearly smooth and lowest in energy at the highest spin values, $I = 19.5 - 25.5$. However, the lower spin values are calculated lower in energy than suggested from a smooth extrapolation from the higher spin states. This feature can be understood from the energy surfaces presented in Figs. 5 and 6.

These surfaces show that for high spin values, the lowest energy for the $[3_+3_+, 21_+0]$ configuration corresponds to a shape at γ-values around $-60°$ or even smaller, i.e. rotation around the longest principal axis. However, for spin values up to $I = 17.5$, the lowest minimum corresponds to positive γ values, i.e. rotation around the shortest principal axis. If instead the negative γ minimum is followed for $I = 17.5$ and below, the energy for the configuration in Fig. 5 comes out as in the middle panel of Fig. 7, i.e. a rather smooth curve which essentially follows the curve for the signature $\alpha = 1/2$ configuration $[3_+3_+, 21_-0]$, where the negative γ minimum is lowest in energy in the spin range $I = 14.5 - 26.5$, see Fig. 6.

Another alternative configuration is $[3_-3_+, 21_+0]$ for total signature $\alpha = 1/2$. The lowest energy minimum of this configuration is found at negative γ values for $I \geq 41/2$. Furthermore, similar to the surfaces in Fig. 5, a minimum at negative γ values can be followed for lower signatures leading to bands with both reasonably continuous deformation changes and bands which are rather
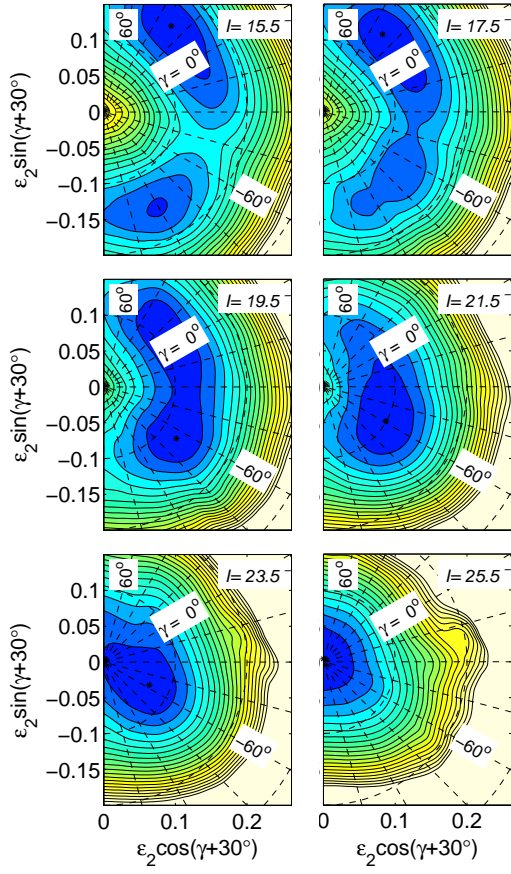
FIG. 5: (Color online) Calculated total energy surface plots for ^{89}Zr for the $[3_+3_+, 21_+0]$ configuration. The contour line separation is 0.25 MeV.
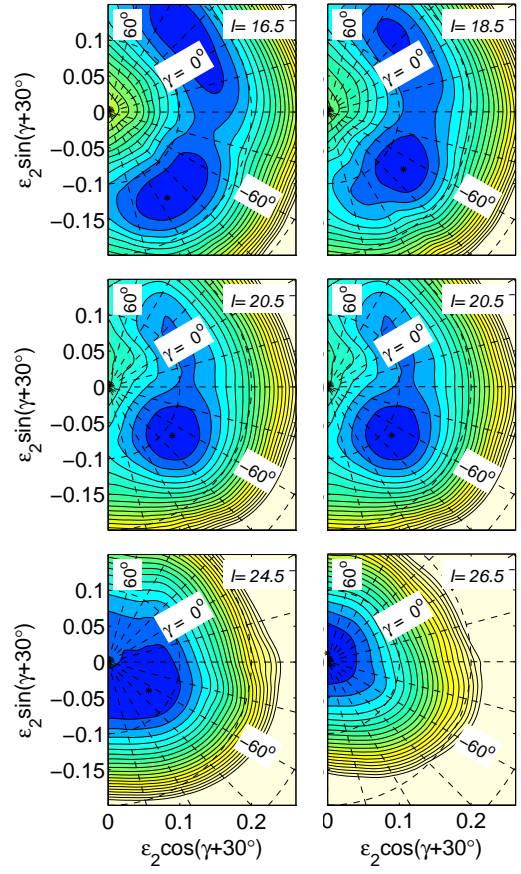

FIG. 6: (Color online) Calculated total energy surface plot for ^{89}Zr for $[3_+3_+, 21_-0]$ configuration. The contour line separation is 0.25 MeV.

close to signature degenerate. Note also that by allowing for a tilted-axis rotation, signature is no longer a preserved quantum number, i.e. the different signatures will mix.

In Fig. 7, the calculated $[3_+3_+, 21_\pm0]$ configurations in the middle panel are compared with the observed band shown in the upper panel. The same rotating liquid drop energy reference is substracted from the experimental level energies in the top panel and from the calculated energies in the middle panel. Both the observed and calculated energies show a characteristic down-slope when drawn versus the rotating liquid drop reference leading to a difference shown in the lower panel which is relatively constant supporting the present assignment.

In the difference curve in the lower panel of Fig. 7, the lowest and highest spin states show some discontinuity. The one at low spin is not unexpected because, also in experiment, there is a discontinuity suggesting that the $I = 14.5$ (and 15.5) states do not belong to the band. The discontinuity at high spin is somewhat more interesting, where Fig. 8 is drawn to illustrate how the signature splitting at termination can be understood.

This is a sloping Fermi surface diagram drawn at a deformation corresponding to an approximate average for the two terminating states. For the protons, we find that with present parameters, signature $\alpha = +1/2$ is clearly favored for the fp as well as for $g_{9/2}$ protons.

For the neutrons, the sloping Fermi surface with two $g_{9/2}$ holes in Fig. 8 indicates that the two signatures for the dg neutron should be degenerate, even though the detailed calculations presented in Fig. 7 show that the configuration with an $m = 5/2$ particle is slightly more favored than the one with a $m = 7/2$ particle. Note however that the splitting at termination is mainly governed by the splitting between the $d_{5/2}$ and $g_{7/2}$ subshells which is associated with rather large uncertainties. We may also note from Fig. 8 that with present parameters and two $g_{9/2}$ holes, the configuration with the excited neutron in $h_{11/2}$ will be about as favored as those shown in Fig. 7 with a dg proton. The corresponding total configuration is however not seen in Fig. 4 because it has positive parity. However, with one more proton excited across the $N = 40$ gap, the corresponding $[44,201]$ configuration is calculated to terminate close to yrast at $I = 31.5$, see Fig. 4.
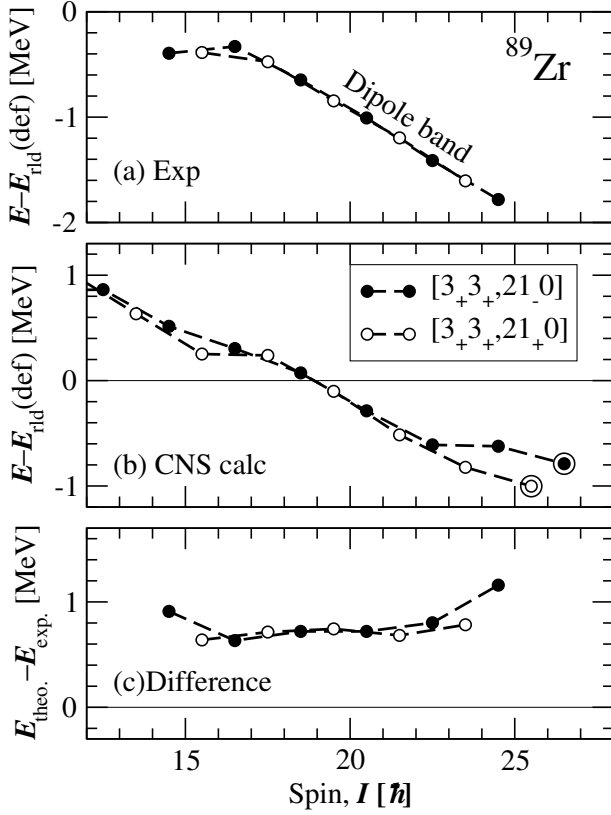
FIG. 7: (panel a) Excitation energies relative to a rotating liquid drop w.r.t. spin for the observed negative parity dipole band. (panel b) Calculated energies relative to a rotating liquid drop energy as a function of spin for the configurations $[3_+3_+, 21_\pm 0]$, where the minimum at negative γ-values is followed, cf. Figs. 5 and 6. (panel c) The difference between experiment and calculations.

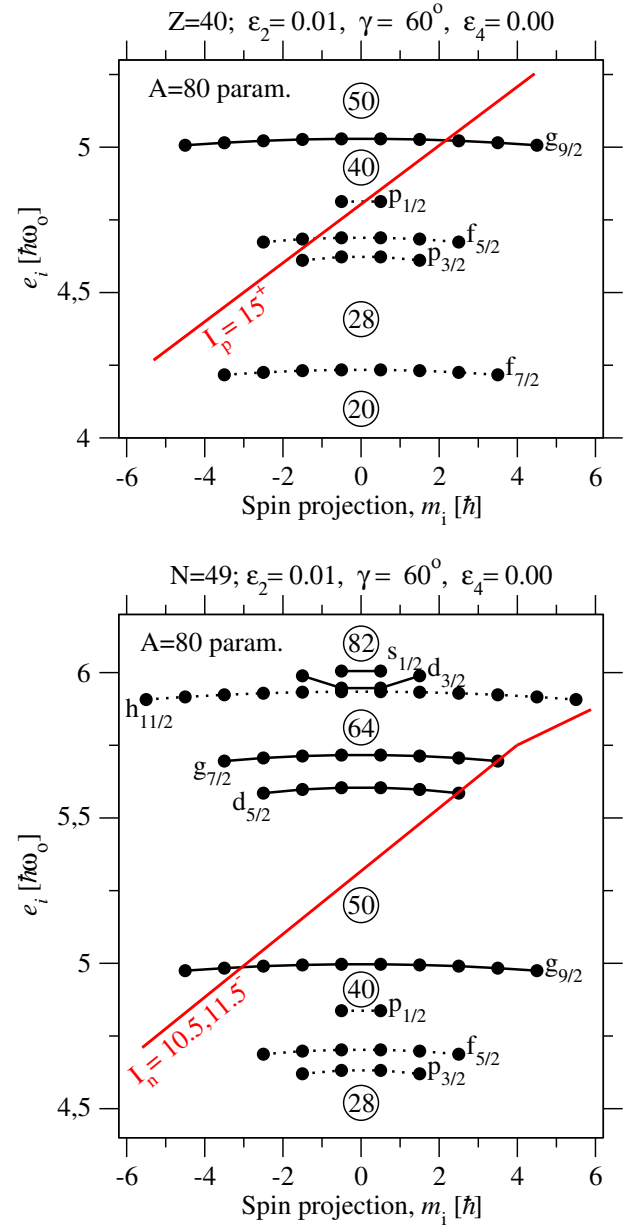

FIG. 8: (Color online) Sloping Fermi surface plot illustrating the maximum spin state in the [33,210], i.e. the $\pi((fp)^{-3} g_{9/2}^3) \otimes \nu(g_{9/2}^{-2}(dg)^1)$ configuration in ^{89}Zr. The total spin is specified for the proton and neutron configurations where all single-particle states below the sloping Fermi surfaces drawn by red lines are occupied. The fact that the neutron Fermi surface with two $g_{9/2}$ holes goes through the $m = 5/2$ and $m = 7/2$ dg states indicates that the neutron configurations with one or the other of these orbitals occupied are about equally favored in energy.

The evolution of shape can also be understood in the framework of distribution of particles and holes in the valence orbitals. When particles align along one of the axes, the matter gets concentrated around the corresponding equator. The alignment of holes reduces the matter density in equator favoring rotation along the longest principal axis. The configuration [33,21] in ^{89}Zr is rich in number of holes and therefore is a likely candidate to be characterized by rotation along the longest axis.

Similar observations were made in ^{142}Gd ($Z = 64$, $N = 78$) by Carlsson et al. [44] where the three minima for rotation around the three principal axes show up very clearly in the calculations. One of the minima at $\gamma \sim -75^0$ represents the rotation around the longest axis. It is instructive to consider the analogy between the valence orbitals for the [33,210] configuration of ^{89}Zr and the $\pi(h_{11/2})^4 \nu(h_{11/2})^{-2}$ configuration of ^{142}Gd. Note that the configurations are very similar but they occur 'one shell higher up' in ^{142}Gd which means that some more valence particles are active in ^{142}Gd. Furthermore, the neutron configuration is a pure hole configuration in ^{142}Gd while one particle is excited across the shell gap in ^{89}Zr. This means that the minimum for rotation around the longest principal axis is somewhat better developed in ^{142}Gd than in ^{89}Zr.

In spite of the analogous shape effects in two mass re-

gions, the band with large negative γ deformation value in ^{142}Gd is a band with $E2$ transitions, whereas the one under present study is a dipole band. This is partly understood from the somewhat smaller deformation in ^{89}Zr, leading to smaller $B(E2)$-values. Furthermore, it seems likely that the rotation axis is tilted in ^{89}Zr leading to stronger $M1$-transitions. As discussed e.g. in Ref. [45], this will only have a minor effect on the energies but lead to an increased $M1$ transition strength.

V. CONCLUSIONS

A regular dipole band, with enhanced $M1$ transition rates has been observed at high spin in ^{89}Zr. Spins and parities of some of the levels of the band have been determined through measurement of DCO ratios and polarisation asymmetries of γ rays. Possible configurations of the band are discussed within a framework of cranked Nilsson Strutinsky model. The calculations show that the lowest energy configuration which can explain the observed band is with three protons excited to $g_{9/2}$ orbitals together with the excitation of one neutron across the N=50 shell gap to gd shells, i.e. [33, 210]. Detailed calculations show that the degenerate band may belong to $[3_+3_+, 21_\pm 0]$ configurations where the band represents

different signatures of gd neutron orbitals. These configurations remain yrast for most of the observed spin range with $\gamma \simeq -60°$ with $\varepsilon_2 \sim 0.1$ and, hence, represents a rotation of a weakly deformed triaxial nucleus rotating about the longest axis. Observation of a dipole band in a nucleus in this mass region with well known spherically symmetric ground state is interesting in this mass region. Similar observations have been made in near-spherical ^{142}Gd nucleus in mass 150 region. However, a difference between these two nuclei is the absence of the $E2$ crossovers in ^{89}Zr. The enhancement of $M1$ transition rates may be due to tilted axis rotation.

VI. ACKNOWLEDGMENTS

[1] E. Ideguchi et al. Phys. Rev. Lett. **87** 222501 (2001).
[2] D. Rudolph et al. Phys. Rev. Lett. **82** 3763 (1999).
[3] A. P. Zuker et al. Phys. Rev. C **52**, R1741 (1995).
[4] A. V. Afanasjev and I. Ragnarsson. Nuclear Physics A **586**, 377 (1995).
[5] M. Ciemala et al., Acta Phys. Polonica B **42**, 633 (2011).
[6] E. A. Stefanova et al., Phys. Rev. C **62**, 054314 (2000).
[7] G. Winter, R. Schwengner, J. Reif, H. Prade, L. Funke, R. Wirowski, N. Nicolay, A. Dewald, P. von Brentano, H. Grawe, and R. Schubart, Phys. Rev. C **48**, 1010 (1993).
[8] L. Funke **et al.** Nuclear Physics A **541**, 241 (1992).
[9] S. Saha et al., Phys. Rev. C **86**, 034315 (2012).
[10] R. Palit, in *Application of Accelerators in Research and Industry: Twenty-First International Conference*, edited by F. D. McDaniel and B. L. Doyle, AIP Conf. Proc. No. 1336 (AIP, New York, 2011), p. 573.
[11] R. Palit et al., Nucl. Instrum. Methods A **680**, (2012) 90.
[12] R. Palit and S. Saha, Pramana, **82** (2014) 649.
[13] A. Krämer-Flecken, T. Morek, R.M. Lieder, W. Gast, G. Hebbinghaus, H.M. Jäger, W. Urban, Nucl. Instrum. and Methods A **275** 333 (1989).
[14] K. S. Krane, R. M. Steffen and R. M. Wheeler, Nuclear Data Tables, **11**, 351-406 (1973).
[15] P. M. Jones et al. Nucl. Instrum. Methods A **362**, 556 (1995).
[16] Lawrence W. Fagg and Staney S. Hanna, Rev. Mod. Phys. **31**, 711 (1959).
[17] K. Starosta et al., Nucl. Instrum. Methods A **423**, 16 (1999).
[18] S. Saha et al., Phys. Rev. C **89**, 044315 (2014).
[19] J. C. Wells and N. R. Johnson, "LINESHAPE: A Computer Program for Doppler-Broadened Lineshape Analysis "
[20] L. C. Northcliffe and R. F. Schilling, Nucl. Data Tables **7**, 233 (1970).
[21] R. Schwengner et al., Phys.Rev.C **57**, 2892 (1998).
[22] F. James and M. Roos, Comput. Phys.Commun. **10**, 343 (1975).
[23] T. Trivedi et al., Phys. Rev. C **85**, 014327 (2012).
[24] M. Honma, T. Otsuka, T. Mizusaki and M Hojorth-Jensen, Phys. Rev. C **80**, 064323 (2009).
[25] M. Honma, T. Otsuka, B. A. Brown, T. Hizusaki Phys. Rev. C **65**, 061301 (2002).
[26] B. A. Brown and A. F. Lisetski (unpublished).
[27] J. J. Liu et al., Eur. Phys. J. A **50**, 84 (2014).
[28] S. E. Arnell et al., Physica Scripta. **46**, 389 (1992).
[29] D. P. Ahalpara and S. P. Pandya, J. Phys. G **12**, 15, (1986).
[30] D.R. Inglis, Phys. Rev. **96**, 1059 (1954); Phys. Rev. **103**, 1786 (1956).
[31] R. Bengtsson and S. Frauendorf, Nucl. Phys. A **327**, 139 (1979).
[32] S. G. Nilsson, Mat. Fys. Medd. Da. Vid. Selsk., **29** 1 (1955).
[33] T. Bengtsson and I. Ragnarsson, Nucl. Phys. A **436**, 14 (1985); A. V. Afanasjev and I. Ragnarsson, Nucl. Phys. A **591**, 387 (1995).
[34] I. Ragnarsson, Phys. Lett. B **264**, 5 (1991).
[35] A. V. Afanasjev, D. B. Fossan, G. J. Lane, and I. Ragnarsson, Phys. Rep. **322**, 1 (1999).
[36] B. G. Carlsson and I. Ragnarsson, Phys. Rev. C **74**,

011302(R) (2006).

[37] S. G. Rohozinski, Phys. Rev. C **56**, 165 (1997).

[38] K. Pomorski and J. Dudek, Phys. Rev. C **67**, 044316(R) (2003).

[39] D. Galeriu et al., J Phys. G, Nucl. Phys. **12**, 329 (1986).

[40] J. Pavan et al., Phys. Rev. C **67**, 034316 (2003).

[41] M. Wiedeking et al., Phys. Rev. C **67**, 034320 (2003).

[42] R. Cardona et al., Phys. Rev. C **68**, 024303 (2003).

[43] B.G. Carlsson and I. Ragnarsson, Phys. Rev. C **70**, 024303 (2004).

[44] B. G. Carlsson, I. Ragnarsson, R. Bengtsson, E. O. Lieder, R. M. Lieder, and A. A. Pasternak, Phys. Rev. C **78**, 034316 (2008).

[45] T. Zerrouki et al., Eur. Phys. J. **A** 51, 50 (2015).